Increasing meteorological drought under climate change reduces terrestrial ecosystem productivity and carbon storage

Zhaoqi Zeng[1,2], Wenxiang Wu[1,3]*, Yamei Li[3], Chong Huang[1], Xueqin Zhang[1], Josep Peñuelas[4,5]*, Yao Zhang[6], Pierre Gentine[7], Zhaolei Li[8], Xiaoyue Wang[1], Han Huang[1,2], Xinshuai Ren[1,2], and Quansheng Ge[1]*

[1]Key Laboratory of Land Surface Pattern and Simulation, Institute of Geographic Sciences and Natural Resources Research, Chinese Academy of Sciences, Beijing 100101, China;

[2]Department of Environment and Resources, University of Chinese Academy of Sciences, Beijing 100049, China;

[3]State Key Laboratory of Tibetan Plateau Earth System, Environment and Resources (TPESER), Institute of Tibetan Plateau Research, Chinese Academy of Sciences, Beijing 100101, China;

[4]CSIC, Global ecology Unit CREAF-CSIC-UAB, Bellaterra 08193, Catalonia, Spain;

[5]CREAF, Cerdanyola del Vallès 08193, Catalonia, Spain;

[6]Sino-French Institute for Earth System Science, College of Urban and Environmental Sciences, Peking University, Beijing, China;

[7]Department of Earth and Environmental Engineering, Center for Learning the Earth with Artificial intelligence and Physics, Columbia University, New York, NY, USA;

[8]College of Resources and Environment, and Academy of Agricultural Sciences, Southwest University, Chongqing 400715, China;

*Correspondence to: W.X. Wu, wuwx@igsnrr.ac.cn; J. Peñuelas, Josep.Penuelas@uab.cat; Q.S. Ge, geqs@igsnrr.ac.cn

Abstract: The terrestrial biosphere absorbs about 30% of the carbon dioxide emitted by human activities each year, playing an important role in regulating global carbon budgets. The persistence of such a carbon sink, however, critically depends on vegetation responses to future increases in atmospheric aridity, decreases in soil water availability, and greater perturbations associated with meteorological droughts under global warming. While the evidence for increasing frequency and intensity of meteorological drought is growing, their potential systematic adverse impacts on vegetation productivity for the coming decades have not been quantified. Using newly-released data from 13 Sixth Coupled Model Intercomparison Project (CMIP6) models and basing on multiple meteorological drought indices, we show that the global mean drought-associated reductions in gross primary productivity (GPP) and net primary productivity (NPP) are projected to increase by 3.5-fold ($p < 0.01$) under the SSP5-8.5 scenario and by 2.3-fold ($p < 0.01$) under the SSP1-2.6 scenario during the period from 2076 to 2100 relative to the historical baseline period (1851–2000). Especially, the terrestrial carbon costs due to meteorological drought increase faster than the mean vegetation productivity enhanced by CO_2 fertilization effect in tropical and temperate ecosystems and particularly for cropland. Increased potential evapotranspiration in response to global warming (i.e., radiative effects of rising CO_2) is likely to play either a dominant and direct role in increasing drought-associated reductions in GPP and NPP, by intensifying meteorological droughts, or an indirect role, by increasing the sensitivity of vegetation productivity to fluctuations in precipitation, or both. Our results indicate that the exacerbation of meteorological droughts under future warming scenarios increase a pressure on global food security and raise the concerns about the transformation of terrestrial ecosystem from a carbon sink into a carbon source.

Keywords: meteorological drought; vegetation productivity; CMIP6; global warming

Introduction

As a key component of the terrestrial carbon cycle and ecosystem process, terrestrial ecosystem production uniquely involves ecological, climatic, and anthropogenic impacts on the global carbon cycle.[1–3] Its alternation, in either magnitude or trend, could profoundly affect CO_2 exchange between the land and the atmosphere, with great implications for the global climate.[4,5] For example, terrestrial C uptake removed about 3.61 Pg of C from the atmosphere annually primarily driven by the acceleration of plants' photosynthesis and water use efficiency in response to the increased concentration of CO_2 (i.e., physiological effects of CO_2) during the period from 2007 to 2016. This accounts for 33.7% of total anthropogenic C emissions from industrial activity and land-use change[5] and thus provides an important negative climate-C feedback. However, there is increasing evidence that the greater atmospheric water demand with rising temperatures (i.e., radiative effects of CO_2) may lead to an increased intensity and frequency of meteorological drought,[6] which could notably affect vegetation growth[7–9] and crop yields,[10] and even drive widespread forest mortality.[11,12] In particular, hotter droughts are an inciting factor in C sinks reduction from insects and may also increase the frequency, size, and intensity of forest fires,[13,14] and thus bring about an associated release of C to the atmosphere that may further accelerate the rate of climate warming through a positive climate-C cycle system feedback loop. Given the increased likelihood of both negative and positive feedback effects of rising levels of CO_2 under future climate conditions, it has been remained an internationally concerned issue of whether future increasing meteorological droughts under continuous global warming will lead to systematic adverse shifts in vegetation productivity at regional and global scales? An improved projection of future drought impacts on terrestrial ecosystem productivity is thus essential to reduce uncertainties in predicting land C uptake and to better understand atmosphere–biosphere interactions.

Precisely quantifying the development of meteorological drought is one of the prerequisites to effective assessment of drought impacts, yet it remains methodologically challenging as using different drought indices to calculate drought characteristics can introduce different uncertainties and even produce apparently conflicting results.[15,16] For example, the Standardized Precipitation Index (SPI) proposed by Mckee, et al.[17] has increasingly been used due to its simplicity and versatility.[18,19] However, the SPI bases only on precipitation data and does not consider other critical variables (e.g., temperature and evapotranspiration) that can markedly influence droughts, the drying trends quantified by the SPI may thus be underestimated under global warming. Alternatively, the Standardized Precipitation Evapotranspiration Index (SPEI_PET-RC), calculated as the difference between precipitation and potential evapotranspiration (PET) that commonly estimated by using reference crop Penman–Monteith equation (PET-RC),[20,21] could better capture the drought dynamics than the SPI especially for regions with substantially higher temperature. However, recent studies suggested that reference crop Penman–Monteith equation prescribed a constant surface resistance (r_s) at 70 s m^{-1}, which is appropriate for an idealized reference crop in the current climate but does not account for the fact that r_s increases with elevated CO_2 over vegetated surfaces in climate model projections.[22–24] Drought projections based on SPEI_PET-RC may thus be overestimated due to the overrated PET under the background of continuously enhanced atmospheric CO_2 concentration. Despite their individual uncertainties, both SPI-based and SPEI_PET-RC-based drought projections may set a lower and upper limit, respectively, for the future drying trend. Given the inherent limitations of any single drought index,[15,25] a multi-index evaluation could better quantify meteorological drought events and provide more important information for understanding the changes in future meteorological drought characteristics and its main causes and impacts.

Drought impacts on vegetation productivity has been examined extensively, but most studies were limited to a regional scale and/or focused on past few decades.[7,26] A recent study produced a global map of long-term projected impacts of soil moisture deficits on vegetation productivity, and suggested that the magnitude of vegetation productivity reduction associated with extreme low soil moisture will increase dramatically.[27] This study provides a preliminary understanding of future drought impacts on vegetation productivity at the global scale. But soil moisture only reflects the amount of water resources available in the underground part of vegetation (root zone), and is thus unable to represent the full influences by other meteorological factors in the aboveground part of vegetation under the drought conditions.[28] Several recent studies indicated that vegetation growth not only suffered from water stress by soil moisture deficit, but also by other meteorological factors, such as extreme high temperature and vapor pressure deficit (VPD).[29–31] Using only soil moisture as drought indicator may thus underestimate the impacts of drought on vegetation productivity in water-limited regions. By contrast, the development of meteorological drought, such as quantified by SPEI, involving interactions between precipitation and temperature that directly controlling the levels of soil moisture and VPD, can more synthetically and accurately capture the response of vegetation growth to drought.[21,32] However, a comprehensive global assessment of projected changes in long-term vegetation productivity response to meteorological droughts is still missing. This knowledge gap prevents a deeper understanding of vegetation response to the expected intensification of drought frequency, severity, and duration under continuous global warming.

In this study, we first create SPEI (including SPEI_PET-RC, which does not take account for the effect of increased CO_2 on PET, and SPEI_PET[CO_2], which does) and SPI, using projection data from 13 state-of-the-art Earth system models (ESMs) in CMIP6, to synthetically characterize and project spatiotemporal variations in meteorological drought characteristics, including frequency, intensity, and duration during the period from 1851 to 2100. We then calculate the difference between modeled and expected GPP and NPP (Figure S1) for each drought month and location, to systematically quantify the drought-associated reduction in GPP and NPP under two contrasting future climate scenarios. We finally use an idealized experiment, in which CO_2 is increased from preindustrial levels by 1% each year only in the atmospheric model (CO_2rad) or in the vegetation model (CO_2phy), or in both (FULL) for four ESMs from the CMIP6 (see Materials and Methods) to specifically assess the individual impacts of radiative and physiological effects of rising CO_2 on projected changes in drought and its associated GPP reduction. Our findings demonstrated that the dominant role of radiative effects of CO_2 in increasing meteorological droughts and its related carbon cost has the great potential to transform terrestrial ecosystem from a carbon sink into a carbon source.

Results

Projected changes in drought characteristics

Under the two future climate scenarios, our analysis indicates that meteorological droughts will become more frequent and longer in duration (Figure 1), particularly after 2025 under the SSP5-8.5 scenario. During the period from 2076 to 2100, drought frequency is projected to increase by 2.58 fold ($p < 0.01$) and 1.55 fold ($p < 0.01$) under the SSP5-8.5 and SSP1-2.6 scenarios, respectively (Figures 1A and 1E), and the mean drought duration is expected to increase by 1.76 ($p < 0.01$) and 0.45 ($p < 0.01$) months (Figures 1C and 1G), respectively, with the longest drought duration being increased by 6.47 ($p < 0.01$) and 2.02 ($p < 0.01$) months (Figures 1D and 1H) per drought event ($p < 0.01$), respectively, compared with the historical period (1851–2000). The levels of drought intensity are also projected to increase significantly ($p < 0.01$) under the two climate scenarios, but after 2075, this increasing trend greatly slows down under the SSP1-2.6 scenario (Figures 1B and 1F). Seasonally, consistent significant ($p < 0.01$) increases in droughts are projected to occur mainly during the boreal winter months of December, January, and February (i.e., summer months for the Southern Hemisphere), with weaker evidence for such increases occurring also in boreal summer months in the Northern Hemisphere and in the latter spring months of November in the Southern Hemisphere (Figure S2). In contrast, the droughts in September and October are projected to decrease for both the

Northern and Southern Hemispheres. By using SPEI_PET[CO_2], we found that the increasing trends in drought frequency, intensity, and duration are generally comparable to that estimated by using SPEI_PET-RC, and all these trends show a significant increase ($p < 0.01$), despite a slight decrease in magnitudes (Figure S3). The increasing trend in these drought characteristics are also notably larger under the SSP5-8.5 scenario than that under the SSP1-2.6 scenario, mainly as the result of the larger increase in PET under the high GHG emission scenario (Figure S4).

Areas where drought frequency is projected to increase significantly ($p < 0.01$) under future climate change are widely distributed across central-southern North America, southwestern Eurasia, western and southern Africa, and much of South America and Australia, which together account for 36.6 and 52.9% of the global land surface (vegetation-covered area) under scenarios SSP1-2.6 and SSP5-8.5, respectively (Figures 2A–B). During the period from 2076 to 2100, drought events are projected to occur biennially on average in most regions listed above under the SSP5-8.5 scenario (Figure S5); at higher latitudes (> 50°N), however, drought frequency is likely to decrease, especially under the low emission scenario. Spatial patterns of drought duration are projected to be similar to those for drought frequency, with significant ($p < 0.01$) increases in 21.9 and 42.3% of the global land surface under the SSP1-2.6 and SSP5-8.5 scenarios, respectively (Figures 2E–F). Drought intensity is projected to exhibit a large increase across nearly all the land surface under the SSP5-8.5 scenario and much smaller in the SSP1-2.6 scenario, with the projected significant ($p < 0.01$) increase in drought intensity areas being decreased from 75.9 to 32.1% of the global land surface. These spatial pattern of drought characteristics are in closer agreement with that indicated by SPEI_PET[CO_2], except for central Africa, where a wetting trend was projected by SPEI_PET[CO_2] under the two future climate scenarios (Figure S6).

In contrast to increases in drought conditions, as indicated by our analyses of the SPEI, water availability is projected to increase (i.e., wetting trends) under the two future climate scenarios, as indicated by analysis of the SPI (Figure S7), notably across northeastern North America and Europe, central-eastern Africa, and much of Asia (Figure S8). Analysis of the SPI also indicates large and long-lasting decreases in water availability across the Amazon Basin, Southern Africa, the southwestern United States, and southwestern Europe, particularly under the SSP5-8.5 scenario. In general, current conditions are expected to intensify (i.e., a tendency for the wet areas to get wetter and dry areas to get drier), as indicated by the SPI, but with no overall effect at the global scale between scenarios SSP5-8.5 and SSP1-2.6 (Figure S8).

Projected changes in sensitivity of vegetation productivity to drought

The magnitudes of total reductions in GPP and NPP associated with SPEI-based drought are projected to increase similarly under the two future climate scenarios (Figure 3), where trends in reduced water availability identified by the SPEI become more pronounced under the SSP5-8.5 scenario than under the SSP1-2.6 scenario. Between the historical (1851−2000) and future (2076–2100) periods, total reductions in the global GPP (NPP) associated with SPEI-based drought are predicted to increase by ~3.5-fold (from 7.49 (5.14) gC m^{-2} $year^{-1}$ to 25.36 (18.24) gC m^{-2} $year^{-1}$; $p < 0.01$) under the SSP5-8.5 scenario and by ~2.3-fold (from 9.73 (6.76) gC m^{-2} $year^{-1}$ to 22.79 (15.67) gC m^{-2} $year^{-1}$; $p < 0.01$) under the SSP1-2.6 scenario. In addition to results based on SPEI at the 3-month timescale, we also used 2-, 4-, 5-, and 6-month timescales of SPEI to evaluate the drought-related GPP reduction under the SSP5-8.5 scenario. The results show great consistency with those from the 3-month SPEI (Figure S9). It should be noted that the projected increase in drought-related reduction in GPP and NPP occurs in the context of future CO_2 fertilization, which would drive an increase in mean vegetation productivity (Figure S1). Therefore, to better understand the drought impacts in relative terms, it is also need to calculate the percentage reductions in GPP and NPP related to meteorological droughts (i.e., ratios of total drought-related reduction in GPP to total modeled GPP in each period). Results indicated that the percentage reductions in GPP, between the 1851−2000 and 2076–2100 periods, are projected to increase from ~0.75 to ~1.96% per year ($p < 0.01$) under the SSP5-8.5 scenario and from ~0.97 to ~1.79% per year ($p < 0.05$) under the SSP1-2.6 scenario (Figure S10A). The drought assessments are not sensitive to the definition of the metrics when using either SPEI_PET-RC or SPEI_PET[CO_2]; the temporal variations in the percentage reduction are highly consistent (Figure S10). These results further indicate a larger increase in C cost resulting from meteorological droughts and the effectiveness of traditional meteorological data-based drought models (i.e., SPEI_PET-RC) in evaluating the drought impacts.

Spatial patterns of areas projected to experience greater drought-related reductions in GPP and NPP during the period from 2076 to 2100 than during the historical period of 1851 to 2000 are correlated well with projected patterns of increased drought frequency, severity, and duration, particularly in southeastern North America, central-eastern South America, southwestern Eurasia, central-southern Australia, and southern Africa (Figure 4). Although meteorological droughts are expected to be more widespread and severe under the SSP5-8.5 scenario, the predicted spatial distribution and changes in drought-associated reductions in GPP and NPP are generally similar under the SSP1-2.6 and SSP5-8.5 scenarios in most temperate regions. In addition, a latitudinal variation in the projected impact of drought on vegetation productivity is clearly revealed, with the greatest reductions in drought-related GPP and NPP for 2076–2100 likely to occur in tropical and temperate regions and the smallest reductions at high latitudes (> 60°N).

Across climate gradients, we found that areas with greater projected changes in drought-related reductions in vegetation productivity (DRP) tend to occur in water-limited (arid) regions, while mean changes in DRP decrease from water- to energy-limited regions and along an aridity gradient, where areas with greater reductions in DRP tend to be concentrated in semiarid ecosystems (0.05 < aridity < 0.5; Figures 5A–B and S11); projected increases in PET are likely to be greater in these arid regions than in humid, energy-limited areas under the SSP1-2.6 and SSP5-8.5 change scenarios (Figure S12). Across plant functional types, the greatest increases in DRP during the period from 2076 to 2100 are projected to occur in cropland, followed by forest and grassland (Figure 5D), whereas within plant functional type, the greatest changes in DRP are likely to occur in the tropics and subtropics (TSGSS, TSMBF, and TSDBF), followed by the temperate regions (TGSS, TBMF, and TCF), and the smallest changes in DRP are likely to occur in the montane and cold regions (MGS, BF, and TUN; Figures 5C and S11).

Despite projected reductions in drought frequency, intensity, and duration, as indicated by the SPI (Figure S7), with greater levels of water availability across the majority of the global land surface, we projected an increased likelihood of drought-related (SPI-based) reductions in GPP and NPP during the period from 2076 to 2100 (Figure S13), predominantly in southwestern North America, southern Africa, northern-central South America, and southwestern Europe (Figure S14). Our analysis demonstrates that SPI indicators of vegetation productivity responses to drought will be more sensitive than those based on the SPEI, indicating that the vegetation productivity will be more sensitive to decreases in precipitation as a result of substantially elevated atmospheric water demand under future climate scenarios, especially for northern China, southwestern Asian, and central Africa (Figure S15). Vegetation drought sensitivity, indicated by the SPEI, will decrease during the period from 2076 to 2100 over more than half of the total vegetated land surfaces, predominantly in the southern hemisphere, and this decrease will be larger under the SSP5-8.5 scenario, suggesting an improvement in drought resistance under the high GHG emission scenario (Figure S15). In addition to SPI and SPEI, we also used soil moisture (SM) as another drought indicator to quantify drought-related GPP (NPP) reduction. These analysis methods are generally consistent with Xu, et al.[27] but used newly released CMIP6 data. Results indicated that SM drought-related GPP (NPP) reduction are predicted to increase from 14.23 (9.52) gC m^{-2} $year^{-1}$ to 40.71 (28.85) gC m^{-2} $year^{-1}$ ($p < 0.01$) under the SSP5-8.5 scenario and from 14.66 (9.85) gC m^{-2} $year^{-1}$ to 29.37 (20.24) gC m^{-2} $year^{-1}$ ($p < 0.01$) under the SSP1-2.6 scenario (Figure S16), which are larger than those quantified by SPEI, especially in the Amazon Basin and the high latitudes (Figure S17).

Mechanisms of projected changes in drought-related reduction in vegetation productivity

With rising atmospheric CO_2 concentrations, plants tend to increase stomatal closure and enhance water use efficiency to minimize water lose, which can induce reduction in transpiration at the leaf level. On the other hand, increased vegetation productivity and leaf biomass due to CO_2 fertilization effects can generate a larger evaporative surface and thus increase transpiration and thus the actual evapotranspiration (ET) at the ecosystem level. By analyzing the projected changes in transpiration and ET in the CO_2phy simulation, we found that both of them show similar spatial patterns and are reduced in about 87% and 74% of the vegetated land surface, respectively, in response to a quadruple increase in CO_2 (Figures 6A and S18). This suggested that extensive leaf area increases are not enough to offset the influence of decreasing stomatal conductance on transpiration and ET. The reduction in ET implies less water vapor available to drive rainfall and more sensible flux to rise surface temperature, which contributes to widespread decrease in precipitation and enhancement in VPD and PET (Figures 6, S18, and S19). These findings collectively indicated that even without the CO_2rad effects, physiological responses alone can also cause a slight meteorological drying (global annual mean SPEI decreased by 0.1), especially for the wet regions (Figure S19). However, the great improvement in water use efficiency (WUE, i.e., GPP/transpiration) can slow down the loss of soil moisture (SM) and protect vegetation from this mild meteorological drying, resulting in little change or even a widespread decrease in drought-related reduction in vegetation productivity, except in the Amazon Basin region (Figure 6C).

In the CO_2rad simulation, despite the fact that 78% of the global land surface experienced an increase in precipitation with a global average increase by 3.87%, this increase is small relative to the enhancement in atmospheric water demand (i.e., VPD and PET), causing a widespread drying trend that indicated by both SM and SPEI (Figure S19). Especially, our results indicated that the spatial patterns of projected changes in precipitation, ET, VPD, SM, and SPEI, as well as the drought-related reduction in vegetation productivity in the full simulation (FULL) are highly consistent with those in the CO_2rad simulation (Figures 6B, 6D, S18, and S19). This further verified that the radiative effects will dominate over the water saving effects of plants' physiology in response to increasing CO_2, resulting in similar surface drying and reduction patterns in climate model simulations with or without the physiologic response. But for some tropical and temperate regions (e.g., Amazon Basin), drought-related GPP reductions are projected to increase in both CO_2phy and CO_2rad simulations, suggesting that the reduction in stomatal conductance due to rising CO_2 and VPD and decrease in SM induced by increasing ET jointly contribute to the larger carbon cost in these regions.

Discussion

Projected changes in drought characteristics

This study provides a comprehensive evaluation of projected changes in meteorological drought characteristics (frequency, intensity, and duration, as indicated by the SPI and SPEI) under low (SSP1-2.6) and high (SSP5-8.5) GHG emission scenarios. The contrasting trends in global mean drought characteristics projected by the analysis of the SPEI and SPI indicate that PET increases more rapidly than precipitation under future climate scenarios, causing an imbalance between water vapor availability and atmospheric demand and thus driving an increase in meteorological drought. The greatest increases in drought conditions will occur predominantly in tropical and subtropical latitudes, with a marked poleward expansion (Figure 2). These findings support the view anticipated by Sherwood, et al.[33] that PET would increase substantially in most tropical and mid-latitude areas in response to global warming, resulting in shifts in local climates to more arid conditions. Chiang, et al.[34] specifically investigated the individual impacts of GHG and aerosol forcing on levels of PET and reported that the negative effects of aerosol forcing may be masked by the positive impacts of GHG forcing in tropical and subtropical regions, which eventually contribute to the increase in PET in these regions. Thus, under anthropogenically induced global warming resulting from an increased concentration of atmospheric CO_2 and other heat-trapping gases, there is a strong expectation of a general increase in PET that is directly related to a greater incidence of drought events with greater severity and longer duration, especially for tropical and subtropical areas.

However, recent studies have indicated that increasing PET driven by global warming may be severely overpredicted in the traditional offline calculations (e.g., the reference crop Penman–Monteith equation), as they neglect the impacts of elevated CO_2 on r_S. When we take the impacts of elevated CO_2 concentration on r_S into account in calculating PET, the projected trends in global mean PET and drought frequency, intensity, and duration still increase significantly ($p < 0.01$), although the magnitudes of these trends show a slight decrease (Figure S3). These findings indicate that the trends in PET can be mostly explained by increased temperature (i.e., radiative effects of rising CO_2) rather than by elevated r_S (i.e., physiological effects of rising CO_2) under rising atmospheric CO_2 concentrations, which is further verified by our mechanism analysis (Figure 6) and is consistent with recent observations.[35] All these results support the premise that the water cycle will intensify in a warming climate because of greater atmospheric water demand.

Future levels of precipitation deficit under anthropogenic climate change, as indicated by the global mean frequency, intensity, and duration of drought events, based on analysis of the SPI, were shown to decrease, inferring that anthropogenic-mediated climate change may not lead to increased droughts as a result of reduced levels of precipitation in most regions. However, our analysis of SPEI data indicates that when they do occur, the extra heat from global warming will increase the rates of evapotranspiration and surface water evaporation, leading to more rapidly occurring drought conditions that are likely to be more intense. In this regard, despite projected increases in precipitation, the anomalous fluctuations in high levels of anthropogenic GHG emissions may also lead to an increased frequency and intensity of meteorological drought conditions. However, because a warmer atmosphere can hold more moisture according to the Clausius–Clapeyron scaling, it is also possible that increasingly intense precipitation under warmer atmospheric conditions may lead to an intensification of moisture levels in currently wet areas, causing a strong tendency for the wetter areas to become wetter under improved levels of anthropogenic GHG emissions (Figure S8).[36–38] This may further exacerbate the problem of uneven distribution of water resources.

Projected changes in drought-reduced productivity

From a C perspective, although the analysis of SPEI data indicated greater increases in the frequency, intensity, and duration of drought under the SSP5-8.5 climate scenario than under the SSP1-2.6 scenario, global mean drought-associated reductions in GPP and NPP tended to be similar (Figures 1 and 3). This paradoxical phenomenon may be explained in two ways. First, the drought resistance of vegetation is improved under the elevated atmospheric CO_2 concentrations (Figure S15). Numerous studies have indicated that rising CO_2 concentrations could stimulate photosynthetic activity[39] and increase intrinsic vegetation water use efficiency with lower stomata conductance,[40] which was also identified by our mechanism analysis (Figure S19). These physiological responses are of particular importance in plant communities subjected to seasonal water shortage or drought conditions, as plants could maintain similar rates of C assimilation with a reduced demand for water.[41] Second, the reduction in GPP (NPP) in drought-sensitive regions may be partially offset by increased vegetation productivity in energy-limited regions during meteorological drought periods. This was verified by our results projecting a substantial increase in vegetation productivity at high latitudes and across some humid regions, such as southeastern China, even during periods of meteorological drought; in particular, these regions were predicted to further expand under the high GHG emission scenario (Figure 4). The increased vegetation productivity during meteorological drought periods indicates that the water limitation caused by drought may not offset the positive effects of higher temperatures and CO_2 concentrations on vegetation growth in these colder and wetter regions, supporting previous studies showing that temperature and photoperiod play more important roles than water availability in vegetation growth at high latitudes.[42,43]

Additionally, the fact that vegetation productivity can increase during drought conditions may also explain why our projected magnitudes of globally averaged reductions in GPP associated with meteorological droughts (25.36 gC m^{-2} $year^{-1}$; i.e., ~2.85 PgC $year^{-1}$) were lower than that estimated by Xu, et al.[27] (~4.7 PgC $year^{-1}$, which is consistent with our estimations by using CMIP6 SM data, i.e., 4.57 PgC $year^{-1}$; Figure S16) during the last quarter of this century under the high GHG emission scenario. As Xu, et al. [27] focused only on the months during which GPP were reduced owing to extreme SM deficit, ignoring the fact that drought is a long-term and gradual developing phenomenon and the responses of vegetation growth to water stress can vary during different drought developing stages. For example, in most energy-limited regions, favorable climate conditions (e.g., enhanced temperature and abundant sunshine) may provide a more important role in promoting vegetation growth during the early drought developing stage, which may partially or even entirely compensate the reduction in GPP caused by extreme SM deficit in the middle or later drought stages.[32,44] In particular, our results indicated that most projected drought events will be initialized by enhanced atmospheric water demand (i.e., PET) due to radiative effects of rising CO_2, which is responsible for the subsequent SM deficits during drought conditions. This further highlight that the impacts of abundant sunshine and increased temperature as well as its tightly related climate factors (e.g., VPD) preceding extreme SM deficit (i.e., during the early drought developing stage) are nonnegligible to comprehensively capture drought-associated reduction in vegetation productivity under climate change.

Overall, continued climate change threatens terrestrial ecosystems far more than it benefits high latitudes. As Penuelas, et al.[45] hypothesized that future increases in global temperature, drought frequency, and key nutrient limitations, such as phosphorous, may drive a shift from one period dominated by the positive effects of atmospheric fertilization on C sink to another characterized by the saturation of these positive effects and a rise in negative impacts on climate change. In terms of drought impacts, our analyses indicate that this transformation has a very high possibility to occur during the period from 2076 to 2100, as the percentage reduction in GPP related to meteorological droughts is projected to increase by a factor of 2 under both the SSP5-8.5 and SSP1-2.6 climate scenarios (Figure S10), suggesting a faster increase in terrestrial C cost resulting from droughts than the mean GPP (NPP) because of CO_2 fertilization effects in the future. But spatially, we highlight that this transformation may be more pronounced across tropical and temperate ecosystems, such as the Amazon, Mediterranean Basin, Southern Africa, and the southwestern United States. This is because larger increases in both SPEI- and SPI-based droughts were projected to occur during the period from 2076 to 2100 in these regions (Figures 2 and S8), indicating a continued rise in atmospheric water demand (PET) under global warming and a decrease in precipitation and associated increase in water limitation that are expected to reduce vegetation productivity in these regions. It is important to note that the optimal air temperature for ecosystem-level GPP, particularly in tropical forests, is close to current growing-season air temperatures but is projected to fall below the actual air temperatures under all future climate scenarios, indicating that temperatures above the optimum may also occur for vegetation productivity in these ecosystems.[29] Thus, the integrated effects of water and temperature limitations associated with both radiative and physiological effects of rising CO_2 may mask the positive impacts of CO_2 fertilization (Figure 6), causing catastrophic impacts on vegetation productivity and thus the transformation of terrestrial ecosystems into C sources in these regions. These predictions of large increases in drought-induced GPP and NPP reductions in tropical and temperate regions support observations of changes in drought-induced vegetation productivity in the Amazon Basin,[46] the western United States,[47] and across the globe (GPP) when using remote sensing-based estimates,[48] implying a further rising threat to the stability of the land C sink. In addition, the largest increases in drought-induced vegetation productivity were projected to occur over croplands (Figure 5C), which may be due to their lower coping capacity in times of water scarcity as compared with woody vegetation with shallower roots and thus more limited access to deeper soil water.[26] Such findings highlight the urge for societies to take actions to reduce increasing pressures of climate change on crop yields and guarantee a global food security.

Uncertainties of predictions and implications for the global C cycle and food security

Several limitations of our study reflect important challenges and open questions. First, many models suffer from substantial tropical sea surface temperature biases that affect the accuracy of the El Niño/Southern Oscillation (ENSO) simulations,[49,50] which would thus affect the reliability of drought event simulations in regions strongly connected to ENSO events; therefore, further research is needed to identify the origins and impacts of these biases. Second, rising temperatures and levels of CO_2 tend to be correlated with regional hydroclimatic conditions,[34,51] and models may not fully capture the vegetation responses to changes in these climate conditions, especially the response of r_s to elevated atmospheric CO_2 in water-limited regions. This merits further attention because the largest increases in meteorological droughts were projected to be concentrated mainly in these water-limited regions. Third, studies of plant physiology have shown that plants have "memory" that allows them to store and recall information from previous events and adjust their responses to future stress conditions accordingly.[52] Future increases in drought frequency may repeatedly trigger a memory of water scarcity in plants and improve their tolerance to extreme drought events, through a reduction in sensitivity.[53] The lack of plant memory effects in CMIP6 models may therefore have led to the overestimation of drought-related reduction in vegetation productivity. In addition to memory effects, droughts elicit legacy effects—multiyear recovery of trees from drought—in plants, which results from the physiological impairment caused by drought-induced water stress.[54,55] Even when climate conditions return to long-term average conditions, surviving trees do not recover their expected growth rates for an average of 2 to 4 years.[56] In CMIP6 models, however, plants' physiological recovery from drought is often assumed to be complete and relatively fast, leading to an underestimation of drought-related GPP (NPP) reduction. Finally, we suggested that the increasing drought-related GPP (NPP) reduction may also be partially compensated for by the positive anomalies of GPP and NPP related to favorable wetness, temperature and radiation, and enhanced water-use efficiency, especially at high latitudes, resulting in increased GPP and NPP, including in drought periods. However, this projection may be too optimistic because the current CMIP6 models do not explicitly consider insect dynamics,[27] which are driven by temperature and drought and that contribute to tree mortality and C cycles at a range of scales.[57,58] Thus, further attention to including these physiological and wider ecosystem processes in future models will lead to an improved understanding of the effects of global change on GPP (NPP) and C cycles.

Conclusions

Compared with historical (1851–2000) levels, CMIP6 models project that the global mean SPEI-based drought frequency, intensity, and duration will significantly increase during the period from 2076 to 2100 under high (SSP5-8.5) and low (SSP1-2.6) future GHG emission scenarios, whereas SPI-based drought hazards are likely to decrease. These contrasting trends highlight the dominant role of PET (i.e., radiative effects of rising CO_2) in the occurrence of drought events for most regions under global warming, which are further verified by mechanism experiments. The projected drought-associated reduction in GPP and NPP (DRP) increased under the two climate scenarios, regardless of the drought indicator (SPI, SPEI), indicating that vegetation productivity will become more sensitive to precipitation fluctuations under enhanced atmospheric water demand. Areas with the greatest increases in DRP are likely to occur in cropland, highlighting the potential threat of meteorological drought to global food security. Spatially, larger DRP areas are projected to concentrate in the tropical and temperate regions, including the Amazon Basin, Southern Africa, the southwestern United States, and Europe, with smaller DRP occurring at high latitudes, where GPP (NPP) even increased during meteorological drought periods. Such spatial patterns of drought and DRP are driven by tradeoffs among the effects of water, temperature, and rising CO_2 concentrations. Improved quantification of the individual and combined impacts of these climate factors on vegetation growth will lead to more reliable projections of ecosystem productivity and thus a better understanding of atmosphere–biosphere feedbacks under future global climate change.

Materials and Methods

CMIP6 model data

We used monthly historical (1850–2014) and future (2015–2100) precipitation, maximum temperature, minimum temperature, relative humidity, wind speed, shortwave radiation, GPP, and NPP data derived from the CMIP6 simulations. At the time of writing this paper, there were 13 earth system models that produced these data (Table S1; https://esgf-node.llnl.gov/projects/cmip6/). Data were bilinearly interpolated to a spatial resolution of 0.5°

× 0.5°. In contrast to CMIP5, CMIP6 data employ a shared socioeconomic pathways (SSPs) framework that describes five alternative evolutions of future society in the absence of climate change or climate policy (SSP1 to SSP5),[59] among which SSP1 and SSP5 envision contrasting trends for human development, as they assume an increasing shift toward sustainable practices (SSP1) and an energy-intensive, fossil-based economy (SSP5). On the basis of assumptions for the SSPs, combined with four representative concentration pathways (RCPs), CMIP6 generates four radiative forcing pathways (SSP1-2.6, SSP2-4.5, SSP3-7.0, and SSP5-8.5) with associated warming to the end of the 21st century in updated versions of integrated assessment models, which has improved performance in many drought-related aspects than CMIP5, from projecting ecosystem productivity (e.g., GPP and NPP) to hydrological process.[60] In this study, we considered SSP1-2.6 and SSP5-8.5 as two future scenarios, where SSP1-2.6 updates the RCP2.6 pathways and represents a low-ending range of future scenarios, as measured by its radiative forcing pathway (2.6 Wm^{-2} in 2100; low forcing sustainability pathway), whereas SSP5-8.5 stabilizes radiative forcing at 8.5 Wm^{-2} in 2100 and is considered a high radiative forcing scenario.[59] Thus, the SSP1-2.6 and SSP5-8.5 scenarios capture the potential influence of future ranges of GHG emissions on drought impacts under a relatively realistic range of socioeconomic development pathways. Additionally, to include the physiological response of vegetation to rising CO_2 in calculating PET (PET[CO_2]) and the SPEI (SPEI_PET[CO_2]), monthly and latitudinally (0.5°) resolved CO_2 concentration data during the period from 1850 to 2100 under the two climate scenarios were used in our analysis.[61]

To specifically investigate the relative influence of radiative and physiological effects of rising CO_2 on projected changes in drought and its related GPP (NPP) reduction, monthly precipitation, maximum temperature, minimum temperature, relative humidity, wind speed, shortwave radiation, transpiration, actual evapotranspiration (ET), soil moisture (SM), and GPP that outputted in three different simulations with 1% per year CO_2 increases from four

CMIP6 models (BCC-CSM2-MR, CanESM5, CMCC-ESM2, and IPSL-CM6A-LR) were used. The three simulations include: (1) 1% per year increase in CO_2 from pre-industrial to quadruple pre-industrial levels for both radiative and physiological processes (FULL; 1pctCO2 in CMIP6 terminology); (2) same as (1) but the CO_2 increase is only in radiative processes, and is fixed to the pre-industrial level for the physiological processes (CO_2rad; 1pctCO2-rad in CMIP6 terminology); and (3) same as (1) but the CO_2 increase is only in physiological processes, and is fixed to the pre-industrial level for the radiative processes (CO_2phy; 1pctCO2-bgc in CMIP6 terminology). These three simulations thus allow for the partitioning of changes in each water and C cycle flux into two components of CO_2rad and CO_2phy. In each simulation, the change in a field (e.g., ET, VPD, PET, and SPEI) due to increasing CO_2 was calculated as the difference between the average of the last 25 years with that of the first 25 years (Figures S18 and S19). VPD was calculated from temperature and relative humidity; PET was calculated by Penman–Monteith equation (see below); annual SPEI was calculated at a 12-month timescale, and the baseline period for SPEI calculation was set to the first 30 years of the FULL model run for all experiments (including CO_2rad and CO_2phy) in a given model. Before calculation, all monthly original data in each simulation and model were first bilinearly interpolated to a common 0.5° × 0.5° grid.

Observed and reanalyzed data

Monthly precipitation and potential evapotranspiration data for the 1980–2018 period were obtained from the Climatic Research Unit Times Series (CRU-TS) data set to calculate an aridity index, defined as the ratio of mean annual precipitation to PET; the latest version of this database (v. 4.03) covers the period from 1901 to 2018 at a spatial resolution of 0.5° × 0.5° over land surfaces (https://data.ceda.ac.uk/badc/cru/data/cru_ts). This data set, which has been widely used in previous studies of climate change,[62,63] was generated from interpolated monthly climatic anomalies derived from more than 4,000 globally distributed meteorological stations.

To characterize the terrestrial ecosystems that were water-limited or energy-limited (see below for specific methods), monthly root-zone soil moisture (SM) and transpiration (trans) data derived from the Global Land Evaporation Amsterdam Model (Gleam v3.3a; https://www.gleam.eu/) were used. Data were generated based on a reanalysis of radiation and air temperature data, a combination of gauge-based, satellite-based, and reanalyzed precipitation data, and satellite-based vegetation optical depth data.[64] Gleam data comprised daily and monthly temporal resolution at 0.25° spatial resolution for the period from 1980 to 2018 and had undergone rigorous correction, preprocessing, and validation.[65] Soil moisture and transpiration data were aggregated to a spatial resolution of 0.5°.

Vegetation distribution data

Vegetation land cover data, based on the International Geosphere–Biosphere Program (IGBP) classification, were extracted from the MCD12Q1 Land Cover Science Data product at a spatial resolution of 0.05° (https://modis.gsfc.nasa.gov/data/dataprod/mod12.php), which were then aggregated to 0.5°.

Changes in drought-related vegetation productivity were quantified by biome type (https://www.worldwildlife.org/publications/terrestrial-ecoregions-of-the-world),[66] which comprise temperate tropical and subtropical moist broadleaf forests (TSMBF), tropical and subtropical dry broadleaf forests (TSDBF), tropical and subtropical coniferous forests (TSCF), temperate broadleaf and mixed forests (TBMF), temperate coniferous forests (TCF), boreal forests or taiga (BF), tropical and subtropical grasslands, savannas, and shrublands (TSGSS), temperate grasslands, savannas, and shrublands (TGSS), flooded grassland and savannas (FGS), montane grasslands and shrublands (MGS), tundra (TUN), Mediterranean forests, woodlands, and scrub (MFWS), deserts and xeric shrublands (DXS), and mangroves (MG). Samples of TSCF (3 pixels) and MG (10 pixels) were limited at a spatial resolution of 0.5°, so they were removed from our analysis (Figure S11).

Definition of drought events and characteristics

Drought events become apparent after substantial periods without precipitation, but quantification of their onset and end times and spatial extent is problematic; as a result, a range of drought indices have been developed.[21] Against the background of rapid global warming, robust drought indices have to include the dynamics of temperature and its closely correlated factors, such as PET. Therefore, we defined drought events in our study based on the SPEI, calculated as the difference between precipitation and PET, to describe drought conditions with respect to normal conditions for a given period.[21] This approach accounts for both the effect of climate warming on drought and the role of land–atmosphere feedback effects in drought development and persistence. It can be calculated for contrasting timescales, where a short-term (e.g., 3-month) SPEI reflects a high frequency of variability in soil moisture that is important for vegetation production, whereas a long-term (e.g., 12-month) SPEI indicates medium-term trends in precipitation and provides annual estimates of water availability that are relevant to hydrological drought. Given that our investigation focused on drought impacts on vegetation productivity, we mainly focus on the 3-month SPEI,[67,68] in which PET (PET-RC) was calculated by the reference crop Penman–Monteith equation[20] (SPEI_PET-RC):

$$\text{PET-RC} = \frac{0.408\Delta(R_n - G) + \gamma(\frac{900}{T_{\mathrm{mean}}+273})U_2(e_s - e_a)}{\Delta + \gamma(1 + 0.34U_2)}, \qquad (1)$$

where R_n is the net radiation at the vegetation surface [MJ·m^{-2}·day^{-1}]; G is the soil heat flux density [MJ·m^{-2}·day^{-1}]; T_{mean} is the mean air temperature at 2 m above ground level [°C]; U_2 is the wind speed 2 m above ground level [m·s^{-1}]; e_s is the saturation pressure of water vapor [kPa]; e_a is the actual water vapor pressure [kPa]; Δ is the slope of the vapor pressure curve [kPa·°C^{-1}]; and, γ is the psychrometric constant [kPa·°C^{-1}]. In the reference crop Penman–Monteith model, the surface resistance (r_s) is prescribed as 70 s m^{-1}, and this parameter value is embedded in the equation.

However, recent studies have suggested that PET and drought conditions may be overestimated by the SPEI_PET-RC, as it does not consider the impact of rising CO_2 on r_s.[22,23] To reduce such uncertainties, we also used a modified reference crop Penman–Monteith PET model that takes the biological effect of elevated [CO_2] into account, as derived by Yuan, et al. [30], to calculate the PET ($\mathrm{PET[CO_2]}$) and SPEI (SPEI_$\mathrm{PET[CO_2]}$). The $\mathrm{PET[CO_2]}$ was calculated as follows:

$$\mathrm{PET[CO_2]} = \frac{0.408\Delta(R_n - G) + \gamma(\frac{900}{T_{\mathrm{mean}}+273})U_2(e_s - e_a)}{\Delta + \gamma\{1 + U_2[0.34 + 2.4\times10^{-4}([CO_2] - 300)]\}}, \quad (2)$$

The monthly SPEI-3 (SPEI at a 3-month timescale) series for each pixel from 1851 to 2100 was calculated to construct the drought duration, intensity, and frequency. The onset and end times of a drought event were defined as the month when the SPEI fell below and returned to −1, respectively. Given that soil moisture stored prior to a drought buffers the impacts on vegetation growth of short-term moisture deficiency, we defined a drought event as occurring just when the SPEI value was less than −1 for at least three consecutive months. Thus, the drought duration was calculated as the number of months between the onset and end of a drought event; the drought intensity was calculated as the mean of monthly SPEI values during the drought period; the drought frequency was defined as the number of drought events that occurred over a specific period. Because the pronounced seasonal shifts in drought can also alter vegetation productivity patterns, monthly and seasonal changes in drought frequency during 2076 to 2100 were also assessed (Figure S2). Additionally, given that the timescales at which different vegetation types respond to drought may differ,[69] in addition to SPEI at a 3-month timescale, we also calculated 2-, 4-, 5-, and 6-month timescales of SPEI to further estimate the projected changes in drought-related GPP reduction under the SSP5-8.5 scenario.

To explore the individual contributions of changes in precipitation and atmospheric water demand (i.e., PET) on long-term trends in drought frequency, intensity, and duration, we also employed the standardized precipitation index (SPI) to define drought events. In contrast to the SPEI, which accounts for precipitation and PET, the SPI accounts for only precipitation. By comparing the results generated by the SPEI and SPI, the individual contributions of precipitation and PET on drought as well as on vegetation productivity can thus be separated. Note that the results generated based SPEI_PET-RC were shown in main text, while results generated based SPEI_PET[CO_2] and SPI were shown in supplementary. In addition to SPEI and SPI, soil moisture (SM) data was used as an additional drought indicator to assess drought impacts. SM drought was defined as the month when SM was below tenth percentiles for the same month during 1851–2000 and caused a decrease in GPP, which is referenced to Xu, et al. [27].

Definition of drought-related reduction in vegetation productivity

We defined drought-related reductions in GPP and NPP (DRP) as a departure in the modeled productivity (CMIP6-exported GPP and NPP data) from the expected productivity (i.e., the theoretical value of GPP and NPP in the absence of drought) during a drought episode:

$$DRP_{mon}(i,j) = EP_{mon}(i,j) - MP_{mon}(i,j), \quad (3)$$

$$DRP_{event}(i,j) = \sum_{m=1}^{DD} DRP_{mon}(i,j), \quad (4)$$

where $DRP_{mon}(i,j)$ is the drought-related reduction in vegetation productivity (i.e., GPP or NPP), $EP_{mon}(i,j)$ is the expected productivity, and $MP_{mon}(i,j)$ is the modeled productivity for a specific drought month mon in a pixel at longitude i and latitude j; $DRP_{event}(i,j)$ is the total reduction during a drought episode, and DD is the duration of a drought event.

To quantify the expected productivity for a given drought month m, a smooth spline ("smooth.spline" function in the R package) was used to fit a smooth curve over noisy simulations of GPP and NPP for m during the period from 1851 to 2100. This method minimizes an objective function that considers the goodness of fit and smoothness of the curve.[27] The difference between the expected and observed productivity for month m during the drought year was defined as DRP_{mon}, with positive values indicating a drought reduction in productivity and negative values indicating the reverse (Equation (2)). Estimation of DRP_{mon} using the smooth spline is described in detail in Figure S1.

For the analysis of temporal global shifts in DRP, we summed $DRP_{event}(i,j)$ across drought events and spatial locations for period p:

$$DRP_{global}(p) = \sum_{j=1}^{Nj} \sum_{i=1}^{Ni} \sum_{f=1}^{Nf} DRP_{event}(i,j,f)\, A(i,j), \tag{5}$$

where Nf is the drought frequency and $A(i,j)$ is the area (m^2) for the pixel at longitude i and latitude j during period p.

Definition of sensitivity of vegetation productivity to drought

Biological sensitivity is the degree to which a system responds to (or is affected by) climate change[70] and is used as a key parameter to quantify the vulnerability of the ecosystem to a climate disturbance.[71] In our study, the sensitivity of vegetation productivity to drought in a pixel for a specific period $Sens_p$ was defined as the mean reduction in productivity per drought unit, defined as the product of the frequency, mean duration, and mean intensity:

$$Sens_p = \frac{\sum_{f=1}^{Nf} DRP_{event}(i,j,f)}{Nf \times D \times I}, \tag{6}$$

where Nf, D, and I represent the drought frequency, mean drought duration, and mean drought intensity, respectively, in a pixel at longitude i and latitude j during period p.

Statistical Analysis

We tested for differences at a specific pixel at longitude i and latitude j in the mean drought frequency, duration, and intensity and drought-related reduction in GPP (NPP) between future periods (2076−2100) and the historical baseline period (1851–2000) by using the Welch two-sample t-test at $p < 0.01$. Temporal trends in mean drought sensitivity were calculated by using the nonparametric Theil–Sen estimator, and pixels in which there were shifts in trend ($p < 0.01$) were identified by using the Mann–Kendall trend test. The dependence of drought-related reduction in GPP (NPP) on climate gradients was tested by a Pearson correlation analysis of annual mean root-zone soil moisture and transpiration (r(SM, trans)), where positive values indicate water-limited conditions and negative values represent energy-limited conditions.[24,72]

Acknowledgments

This research was funded by the Strategic Priority Research Program of the Chinese Academy of Sciences (Grant No. XDA20090000) and the National Natural Science Foundation of China (Grant No. 42271317). J.P.'s research was funded by the Spanish Government (Grant No. PID2019-110521GB-I00), the Catalan Government (Grant No. SGR 2017-1005), the Fundación Ramon Areces (project ELEMENTAL-CLIMATE), and the European Research Council (Synergy Grant No. ERC-SyG-2013-610028, IMBALANCE-P).

Conflict of interest

The authors declare no competing financial interests

References

1. Gatti, L.V., Basso, L.S., Miller, J.B., Gloor, M., Domingues, L.G., Cassol, H.L.G., Tejada, G., Aragao, L.E.O.C., Nobre, C., Peters, W. et al. (2021) Amazonia as a carbon source linked to deforestation and climate change. Nature 595 (7867), 388–393.

2. Qin, Y., Xiao, X., Wigneron, J.-P., Ciais, P., Brandt, M., Fan, L., Li, X., Crowell, S., Wu, X., Doughty, R. et al. (2021) Carbon loss from forest degradation exceeds that from deforestation in the Brazilian Amazon. Nature Climate Change 11 (5), 442–448.

3. Beer, C., Reichstein, M., Tomelleri, E., Ciais, P., Jung, M., Carvalhais, N., Roedenbeck, C., Arain, M.A., Baldocchi, D., Bonan, G.B. et al. (2010) Terrestrial Gross Carbon Dioxide Uptake:

Global Distribution and Covariation with Climate. Science 329 (5993), 834–838.

4. Reichstein, M., Bahn, M., Ciais, P., Frank, D., Mahecha, M.D., Seneviratne, S.I., Zscheischler, J., Beer, C., Buchmann, N., Frank, D.C. et al. (2013) Climate extremes and the carbon cycle. Nature 500 (7462), 287–295.

5. Keenan, T.F. and Williams, C.A. (2018) The Terrestrial Carbon Sink. In Annual Review of Environment and Resources, Vol 43 (Gadgil, A. and Tomich, T.P. eds), pp. 219–243.

6. Dai, A. (2013) Increasing drought under global warming in observations and models. Nature Climate Change 3 (2), 52–58.

7. Jiao, W., Wang, L., Smith, W.K., Chang, Q., Wang, H. and D'Odorico, P. (2021) Observed increasing water constraint on vegetation growth over the last three decades. Nature Communications 12 (1), 3777.

8. Restaino, C.M., Peterson, D.L. and Littell, J. (2016) Increased water deficit decreases Douglas fir growth throughout western US forests. Proceedings of the National Academy of Sciences of the United States of America 113 (34), 9557–9562.

9. Wang, S., Zhang, Y., Ju, W., Chen, J.M., Ciais, P., Cescatti, A., Sardans, J., Janssens, I.A., Wu, M., Berry, J.A. et al. (2020) Recent global decline of CO2 fertilization effects on vegetation photosynthesis. Science 370 (6522), 1295–1300.

10. Lobell, D.B., Roberts, M.J., Schlenker, W., Braun, N., Little, B.B., Rejesus, R.M. and Hammer, G.L. (2014) Greater Sensitivity to Drought Accompanies Maize Yield Increase in the US Midwest. Science 344 (6183), 516–519.

11. Adams, H.D., Zeppel, M.J.B., Anderegg, W.R.L., Hartmann, H., Landhausser, S.M., Tissue, D.T., Huxman, T.E., Hudson, P.J., Franz, T.E., Allen, C.D. et al. (2017) A multi-species synthesis of physiological mechanisms in drought-induced tree mortality. Nature Ecology & Evolution 1 (9), 1285–1291.

12. Williams, A.P., Allen, C.D., Macalady, A.K., Griffin, D., Woodhouse, C.A., Meko, D.M.,

Swetnam, T.W., Rauscher, S.A., Seager, R., Grissino-Mayer, H.D. et al. (2013) Temperature as a potent driver of regional forest drought stress and tree mortality. Nature Climate Change 3 (3), 292–297.

13. Williams, A.P., Allen, C.D., Millar, C.I., Swetnam, T.W., Michaelsen, J., Still, C.J. and Leavitt, S.W. (2010) Forest responses to increasing aridity and warmth in the southwestern United States. Proceedings of the National Academy of Sciences of the United States of America 107 (50), 21289–21294.

14. Flannigan, M.D., Krawchuk, M.A., de Groot, W.J., Wotton, B.M. and Gowman, L.M. (2009) Implications of changing climate for global wildland fire. International Journal of Wildland Fire 18 (5), 483–507.

15. Trenberth, K.E., Dai, A., van der Schrier, G., Jones, P.D., Barichivich, J., Briffa, K.R. and Sheffield, J. (2014) Global warming and changes in drought. Nature Climate Change 4 (1), 17-22.

16. Sheffield, J., Wood, E.F. and Roderick, M.L. (2012) Little change in global drought over the past 60 years. Nature 491 (7424), 435-+.

17. Mckee, T.B., Doesken, N.J. and Kleist, J. (1993) The relationship of drought frequency and duration to time scales. In Proceedings of the 8th Conference on Applied Climatology, Anaheim, CA, USA, 179–183.

18. Gocic, M. and Trajkovic, S. (2014) Spatiotemporal characteristics of drought in Serbia. Journal of Hydrology 510, 110-123.

19. Spinoni, J., Naumann, G., Carrao, H., Barbosa, P. and Vogt, J. (2014) World drought frequency, duration, and severity for 1951-2010. International Journal of Climatology 34 (8), 2792-2804.

20. Allen, R.G., Pereira, L.S., Raes, D. and Smith, M. (1998) Crop evapotranspiration-Guidelines for computing crop water requirements-FAO Irrigation and drainage paper 56. Fao

Roma 300, D05109.

21. Vicente-Serrano, S.M., Begueria, S. and Lopez-Moreno, J.I. (2010) A Multiscalar Drought Index Sensitive to Global Warming: The Standardized Precipitation Evapotranspiration Index. Journal of Climate 23 (7), 1696–1718.

22. Yang, Y., Roderick, M.L., Zhang, S., McVicar, T.R. and Donohue, R.J. (2019) Hydrologic implications of vegetation response to elevated CO2 in climate projections. Nature Climate Change 9 (1), 44–48.

23. Milly, P.C.D. and Dunne, K.A. (2016) Potential evapotranspiration and continental drying. Nature Climate Change 6 (10), 946–949.

24. Berg, A. and McColl, K.A. (2021) No projected global drylands expansion under greenhouse warming. Nature Climate Change 11 (4), 331–371.

25. Ukkola, A.M., De Kauwe, M.G., Roderick, M.L., Abramowitz, G. and Pitman, A.J. (2020) Robust Future Changes in Meteorological Drought inCMIP6Projections Despite Uncertainty in Precipitation. Geophysical Research Letters 47 (11).

26. Gampe, D., Zscheischler, J., Reichstein, M., O'Sullivan, M., Smith, W.K., Sitch, S. and Buermann, W. (2021) Increasing impact of warm droughts on northern ecosystem productivity over recent decades. Nature Climate Change 11 (9), 772–779.

27. Xu, C., McDowell, N.G., Fisher, R.A., Wei, L., Sevanto, S., Christoffersen, B.O., Weng, E. and Middleton, R.S. (2019) Increasing impacts of extreme droughts on vegetation productivity under climate change. Nature Climate Change 9 (12), 948–953.

28. Zheng, F., Ciais, P., Prentice, I.C., Gentine, P. and Hajima, T. (2022) Atmospheric dryness reduces photosynthesis along a large range of soil water deficits. Nature Communications 13 (1), 1234567890.

29. Huang, M., Piao, S., Ciais, P., Penuelas, J., Wang, X., Keenan, T.F., Peng, S., Berry, J.A., Wang, K., Mao, J. et al. (2019) Air temperature optima of vegetation productivity across global

biomes. Nature Ecology & Evolution 3 (5), 772–779.

30. Yuan, W., Zheng, Y., Piao, S., Ciais, P., Lombardozzi, D., Wang, Y., Ryu, Y., Chen, G., Dong, W., Hu, Z. et al. (2019) Increased atmospheric vapor pressure deficit reduces global vegetation growth. Science Advances 5 (8).

31. Grossiord, C., Buckley, T.N., Cernusak, L.A., Novick, K.A., Poulter, B., Siegwolf, R.T.W., Sperry, J.S. and McDowell, N.G. (2020) Plant responses to rising vapor pressure deficit. New Phytologist 226 (6), 1550-1566.

32. Zeng, Z., Wu, W., Ge, Q., Li, Z., Wang, X., Zhou, Y., Zhang, Z., Li, Y., Huang, H., Liu, G. et al. (2021) Legacy effects of spring phenology on vegetation growth under preseason meteorological drought in the Northern Hemisphere. Agricultural and Forest Meteorology 310.

33. Sherwood, S. and Fu, Q. (2014) A Drier Future? Science 343 (6172), 737–739.

34. Chiang, F., Mazdiyasni, O. and AghaKouchak, A. (2021) Evidence of anthropogenic impacts on global drought frequency, duration, and intensity. Nature Communications 12 (1), 2754.

35. Wang, R., Li, L., Gentine, P., Zhang, Y., Chen, J., Chen, X., Chen, L., Ning, L., Yuan, L. and Lu, G. (2022) Recent increase in the observation-derived land evapotranspiration due to global warming. Environmental Research Letters 17 (2).

36. Zhang, X., Zwiers, F.W., Hegerl, G.C., Lambert, F.H., Gillett, N.P., Solomon, S., Stott, P.A. and Nozawa, T. (2007) Detection of human influence on twentieth-century precipitation trends. Nature 448 (7152), 461–465.

37. Min, S.-K., Zhang, X. and Zwiers, F. (2008) Human-induced arctic moistening. Science 320 (5875), 518–520.

38. Seager, R., Naik, N. and Vecchi, G.A. (2010) Thermodynamic and Dynamic Mechanisms for Large-Scale Changes in the Hydrological Cycle in Response to Global Warming. Journal of Climate 23 (17), 4651–4668.

39. Gunderson, C.A. and Wullschleger, S.D. (1994) Photosynthetic acclimation in trees to rising atmospheric CO2: A broader perspective. Photosynthesis Research 39 (3), 369–388.

40. Keenan, T.F., Hollinger, D.Y., Bohrer, G., Dragoni, D., Munger, J.W., Schmid, H.P. and Richardson, A.D. (2013) Increase in forest water-use efficiency as atmospheric carbon dioxide concentrations rise. Nature 499 (7458), 324–327.

41. Driscoll, A.W., Bitter, N.Q., Sandquist, D.R. and Ehleringer, J.R. (2020) Multidecadal records of intrinsic water-use efficiency in the desert shrub Encelia farinosa reveal strong responses to climate change. Proceedings of the National Academy of Sciences of the United States of America 117 (31), 18161–18168.

42. Piao, S., Tan, J., Chen, A., Fu, Y.H., Ciais, P., Liu, Q., Janssens, I.A., Vicca, S., Zeng, Z., Jeong, S.-J. et al. (2015) Leaf onset in the northern hemisphere triggered by daytime temperature. Nature Communications 6, 6911.

43. Berner, L.T., Massey, R., Jantz, P., Forbes, B.C., Macias-Fauria, M., Myers-Smith, I., Kumpula, T., Gauthier, G., Andreu-Hayles, L., Gaglioti, B.V. et al. (2020) Summer warming explains widespread but not uniform greening in the Arctic tundra biome. Nature Communications 11 (1), 4621.

44. Tang, H. and Dubayah, R. (2017) Light-driven growth in Amazon evergreen forests explained by seasonal variations of vertical canopy structure. Proceedings of the National Academy of Sciences of the United States of America 114 (10), 2640-2644.

45. Penuelas, J., Ciais, P., Canadell, J.G., Janssens, I.A., Fernandez-Martinez, M., Carnicer, J., Obersteiner, M., Piao, S., Vautard, R. and Sardans, J. (2017) Shifting from a fertilization-dominated to a warming-dominated period. Nature Ecology & Evolution 1 (10), 1438–1445.

46. Doughty, C.E., Metcalfe, D.B., Girardin, C.A.J., Farfan Amezquita, F., Galiano Cabrera, D., Huaraca Huasco, W., Silva-Espejo, J.E., Araujo-Murakami, A., da Costa, M.C., Rocha, W. et al. (2015) Drought impact on forest carbon dynamics and fluxes in Amazonia. Nature 519

(7541), 78–82.
47. Breshears, D.D., Cobb, N.S., Rich, P.M., Price, K.P., Allen, C.D., Balice, R.G., Romme, W.H., Kastens, J.H., Floyd, M.L., Belnap, J. et al. (2005) Regional vegetation die-off in response to global-change-type drought. Proceedings of the National Academy of Sciences of the United States of America 102 (42), 15144–15148.
48. Zhao, M. and Running, S.W. (2010) Drought-Induced reduction in global terrestrial net primary production from 2000 through 2009. Science 329 (5994), 940–943.
49. McKenna, S., Santoso, A., Sen Gupta, A., Taschetto, A.S. and Cai, W. (2020) Indian Ocean Dipole in CMIP5 and CMIP6: characteristics, biases, and links to ENSO. Scientific Reports 10 (1), 11500.
50. Zhu, Y., Zhang, R.-H. and Sun, J. (2020) North Pacific Upper-Ocean Cold Temperature Biases in CMIP6 Simulations and the Role of Regional Vertical Mixing. Journal of Climate 33 (17), 7523–7538.
51. DeAngelis, A.M., Qu, X. and Hall, A. (2016) Importance of vegetation processes for model spread in the fast precipitation response to CO2 forcing. Geophysical Research Letters 43 (24), 12550–12559.
52. Galviz, Y.C.F., Ribeiro, R.V. and Souza, G.M. (2020) Yes, plants do have memory. Theoretical and Experimental Plant Physiology 32 (3), 195–202.
53. Fang, O., Zhang, Q.-B., Vitasse, Y., Zweifel, R. and Cherubini, P. (2021) The frequency and severity of past droughts shape the drought sensitivity of juniper trees on the Tibetan plateau. Forest Ecology and Management 486, 118968.
54. Bastos, A., Ciais, P., Friedlingstein, P., Sitch, S., Pongratz, J., Fan, L., Wigneron, J.P., Weber, U., Reichstein, M., Fu, Z. et al. (2020) Direct and seasonal legacy effects of the 2018 heat wave and drought on European ecosystem productivity. Science Advances 6 (24).
55. Kannenberg, S.A., Novick, K.A., Alexander, M.R., Maxwell, J.T., Moore, D.J.P., Phillips,

R.P. and Anderegg, W.R.L. (2019) Linking drought legacy effects across scales: From leaves to tree rings to ecosystems. Global Change Biology 25 (9), 2978–2992.

56. Anderegg, W.R.L., Schwalm, C., Biondi, F., Camarero, J.J., Koch, G., Litvak, M., Ogle, K., Shaw, J.D., Shevliakova, E., Williams, A.P. et al. (2015) Pervasive drought legacies in forest ecosystems and their implications for carbon cycle models. Science 349 (6247), 528–532.

57. Lehmann, P., Ammunet, T., Barton, M., Battisti, A., Eigenbrode, S.D., Jepsen, J.U., Kalinkat, G., Neuvonen, S., Niemela, P., Terblanche, J.S. et al. (2020) Complex responses of global insect pests to climate warming. Frontiers in Ecology and the Environment 18 (3), 141–149.

58. Anderegg, W.R.L., Hicke, J.A., Fisher, R.A., Allen, C.D., Aukema, J., Bentz, B., Hood, S., Lichstein, J.W., Macalady, A.K., McDowell, N. et al. (2015) Tree mortality from drought, insects, and their interactions in a changing climate. New Phytologist 208 (3), 674–683.

59. O'Neill, B.C., Tebaldi, C., van Vuuren, D.P., Eyring, V., Friedlingstein, P., Hurtt, G., Knutti, R., Kriegler, E., Lamarque, J.-F., Lowe, J. et al. (2016) The Scenario Model Intercomparison Project (ScenarioMIP) for CMIP6. Geoscientific Model Development 9 (9), 3461–3482.

60. Cook, B.I., Mankin, J.S., Marvel, K., Williams, A.P., Smerdon, J.E. and Anchukaitis, K.J. (2020) Twenty-First Century Drought Projections in the CMIP6 Forcing Scenarios. Earths Future 8 (6), e2019EF001461.

61. Meinshausen, M., Vogel, E., Nauels, A., Lorbacher, K., Meinshausen, N., Etheridge, D.M., Fraser, P.J., Montzka, S.A., Rayner, P.J., Trudinger, C.M. et al. (2017) Historical greenhouse gas concentrations for climate modelling (CMIP6). Geoscientific Model Development 10 (5), 2057–2116.

62. Humphrey, V., Berg, A., Ciais, P., Gentine, P., Jung, M., Reichstein, M., Seneviratne, S.I. and Frankenberg, C. (2021) Soil moisture–atmosphere feedback dominates land carbon uptake variability. Nature 592 (7852), 65–69.

63. Li, X., Piao, S., Wang, K., Wang, X., Wang, T., Ciais, P., Chen, A., Lian, X., Peng, S. and Penuelas, J. (2020) Temporal trade-off between gymnosperm resistance and resilience increases forest sensitivity to extreme drought. Nature Ecology & Evolution 4 (8), 1075–1083.

64. Martens, B., Miralles, D.G., Lievens, H., van der Schalie, R., de Jeu, R.A.M., Fernandez-Prieto, D., Beck, H.E., Dorigo, W.A. and Verhoest, N.E.C. (2017) GLEAM v3: satellite-based land evaporation and root-zone soil moisture. Geoscientific Model Development 10 (5), 1903–1925.

65. Miralles, D.G., De Jeu, R.A.M., Gash, J.H., Holmes, T.R.H. and Dolman, A.J. (2011) Magnitude and variability of land evaporation and its components at the global scale. Hydrology and Earth System Sciences 15 (3), 967–981.

66. Olson, D.M., Dinerstein, E., Wikramanayake, E.D., Burgess, N.D., Powell, G.V.N., Underwood, E.C., D'Amico, J.A., Itoua, I., Strand, H.E., Morrison, J.C. et al. (2001) Terrestrial ecoregions of the worlds: A new map of life on Earth. Bioscience 51 (11), 933–938.

67. Jiang, P., Liu, H., Piao, S., Ciais, P., Wu, X., Yin, Y. and Wang, H. (2019) Enhanced growth after extreme wetness compensates for post-drought carbon loss in dry forests. Nature Communications 10, 195.

68. Wu, C., Wang, J., Ciais, P., Penuelas, J., Zhang, X., Sonnentag, O., Tian, F., Wang, X., Wang, H., Liu, R. et al. (2021) Widespread decline in winds delayed autumn foliar senescence over high latitudes. Proceedings of the National Academy of Sciences of the United States of America 118 (16), e2015821118.

69. Vicente-Serrano, S.M., Gouveia, C., Camarero, J.J., Beguería, S., Trigo, R., López-Moreno, J.I., Azorín-Molina, C., Pasho, E., Lorenzo-Lacruz, J. and Revuelto, J. (2013) Response of vegetation to drought time-scales across global land biomes. Proceedings of the National Academy of Sciences 110 (1), 52-57.

70. Beaugrand, G. (2014) Marine Biodiversity, Climatic Variability and Global Change,

Routledge.

71. Choat, B., Jansen, S., Brodribb, T.J., Cochard, H., Delzon, S., Bhaskar, R., Bucci, S.J., Feild, T.S., Gleason, S.M., Hacke, U.G. et al. (2012) Global convergence in the vulnerability of forests to drought. Nature 491 (7426), 752–755.

72. Berg, A. and Sheffield, J. (2018) Soil Moisture-Evapotranspiration Coupling in CMIP5 Models: Relationship with Simulated Climate and Projections. Journal of Climate 31 (12), 4865–4878.

Figure legends

Figure 1. Temporal changes in SPEI-based (SPEI_PET-RC) drought characteristics from 1851 to 2100 under the SSP5-8.5 (A–D) and SSP1-2.6 (E–H) climate scenarios comprising changes in drought frequency (A, E), mean drought intensity (B, F), mean drought duration (C, G), and mean longest drought duration (D, H). The solid red line represents the overall multi model mean, and the shading represents the mean ± SD.

Figure 2. Spatial patterns of mean changes in drought characteristics, based on SPEI_PET-RC, between future (2076–2100) and historical (1851–2000) periods under the SSP5-8.5 (A, C, E) and SSP1-2.6 (B, D, F) climate scenarios. The stippling denotes regions with changes in mean drought at $p < 0.05$. The insets in A, C, and E represent frequency distributions of mean changes in drought frequency, intensity, and duration, respectively, under the SSP5-8.5 (red line) and SSP1-2.6 (blue line) climate scenarios; vertical lines represent average values. The insets in B, D, and F show proportions (%) of areas with increases (*+) or decreases (*−) in drought frequency, intensity, and duration, respectively, under the SSP5-8.5 (red bar) and SSP1-2.6 (blue bar) climate scenarios at $p < 0.05$.

Figure 3. Temporal changes in the drought-related reduction in vegetation productivity, based on the SPEI_PET-RC, during period from 1851 to 2100 under the SSP5-8.5 (A, B) and SSP1-2.6 (C, D) climate scenarios: drought-related reduction in GPP (A, C) and drought-related reduction in NPP (B, D). The solid red line represents overall multi-model means, and the shading represents the mean ± SD.

Figure 4. Spatial patterns of mean changes in the drought-related reduction in GPP (A, D) and NPP (B, E) between future (2076–2100) and historical (1851–2000) periods under the SSP5-8.5 (A, B) and SSP1-2.6 (D, E) climate scenarios. The stippling indicates regions with mean changes in drought-related GPP and NPP reduction at $p < 0.05$. (C, F) Latitudinal comparison of mean changes in drought-related reduction in GPP (red) and NPP (blue); the solid line

indicates means, and the shading represents the SD.

Figure 5. Dependence of changes in the drought-related reduction in vegetation productivity on climate and vegetation gradients. Boxplots of mean changes in drought-related reduction in GPP (tomato boxes) and NPP (orange boxes) across cor(SM, trans) gradients (A); *+, +, –, and *– for significant (p < 0.05) positive, positive, negative, and significant (p < 0.05) negative values, respectively, where positive values indicate water-limited transpiration and negative values reflect energy limitation. Boxplots of mean changes in the drought-related reduction in GPP (tomato boxes) and NPP (orange boxes) across aridity gradients (B), biome types (C), and plant functional types (D).

Figure 6. Global mean relative changes in precipitation (Pre), transpiration (Tran), actual evapotranspiration (ET), vapor pressure deficit (VPD), potential evapotranspiration (PET), and water use efficiency (WUE), and annual mean values changes in the Standardized Precipitation Evapotranspiration Index (SPEI) between last 25 years with the first 25 years under the FULL, CO_2phy, and CO_2rad simulations (A). Spatial patterns of mean changes in the drought-related reduction in GPP between last 25 years with the first 25 years under the FULL (B), CO_2phy (C), and CO_2rad (D) simulations.

912 **Figure 1**

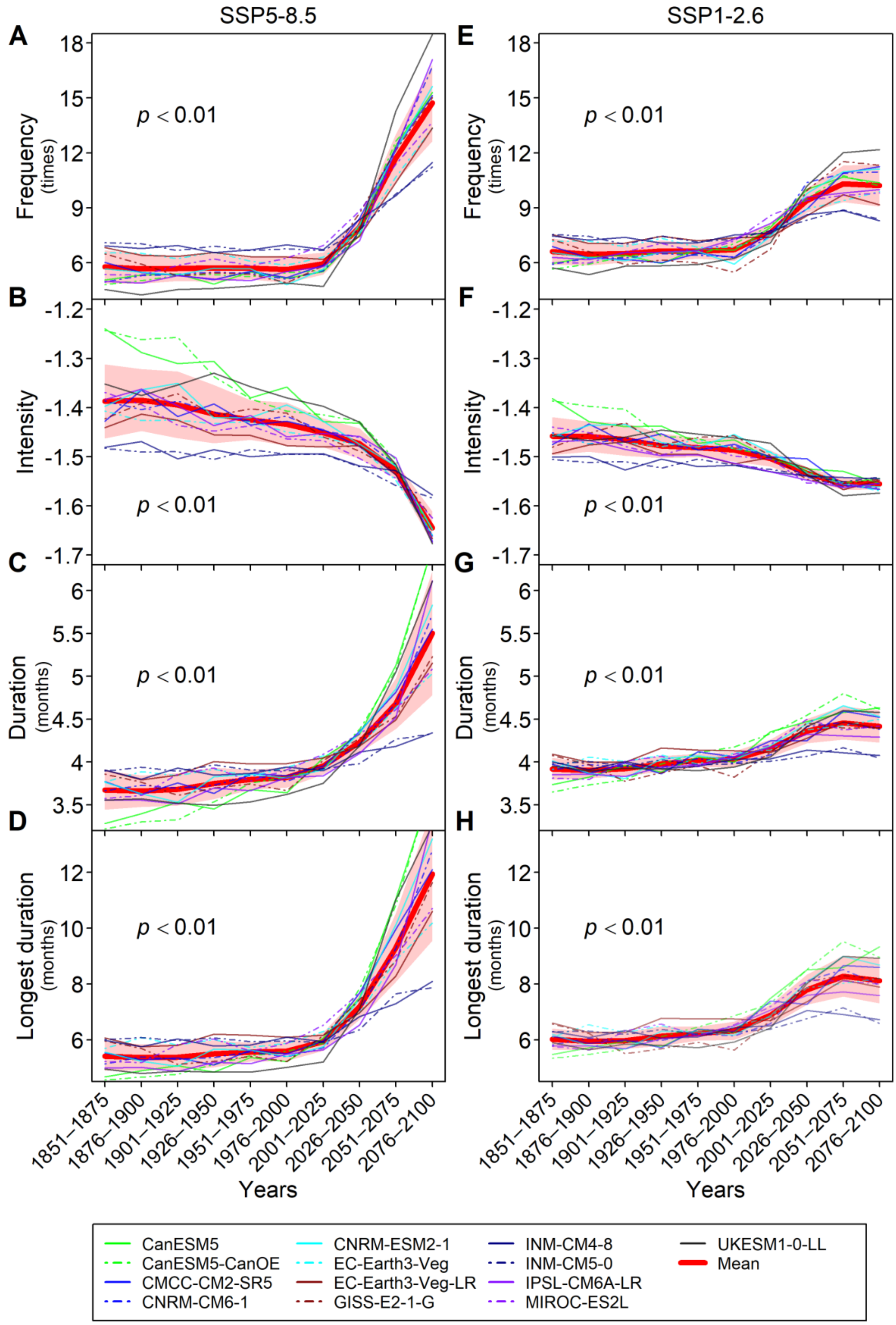

913

914 **Figure 2**

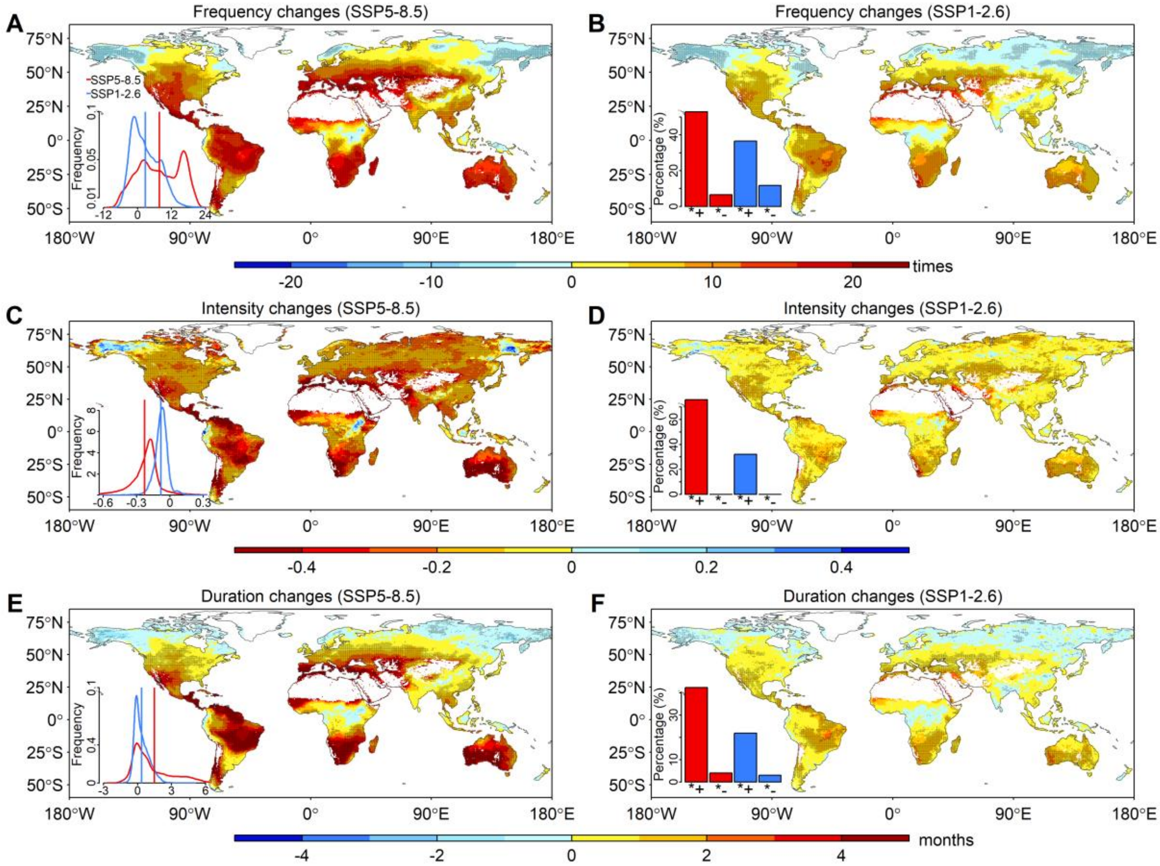

915

916 **Figure 3**

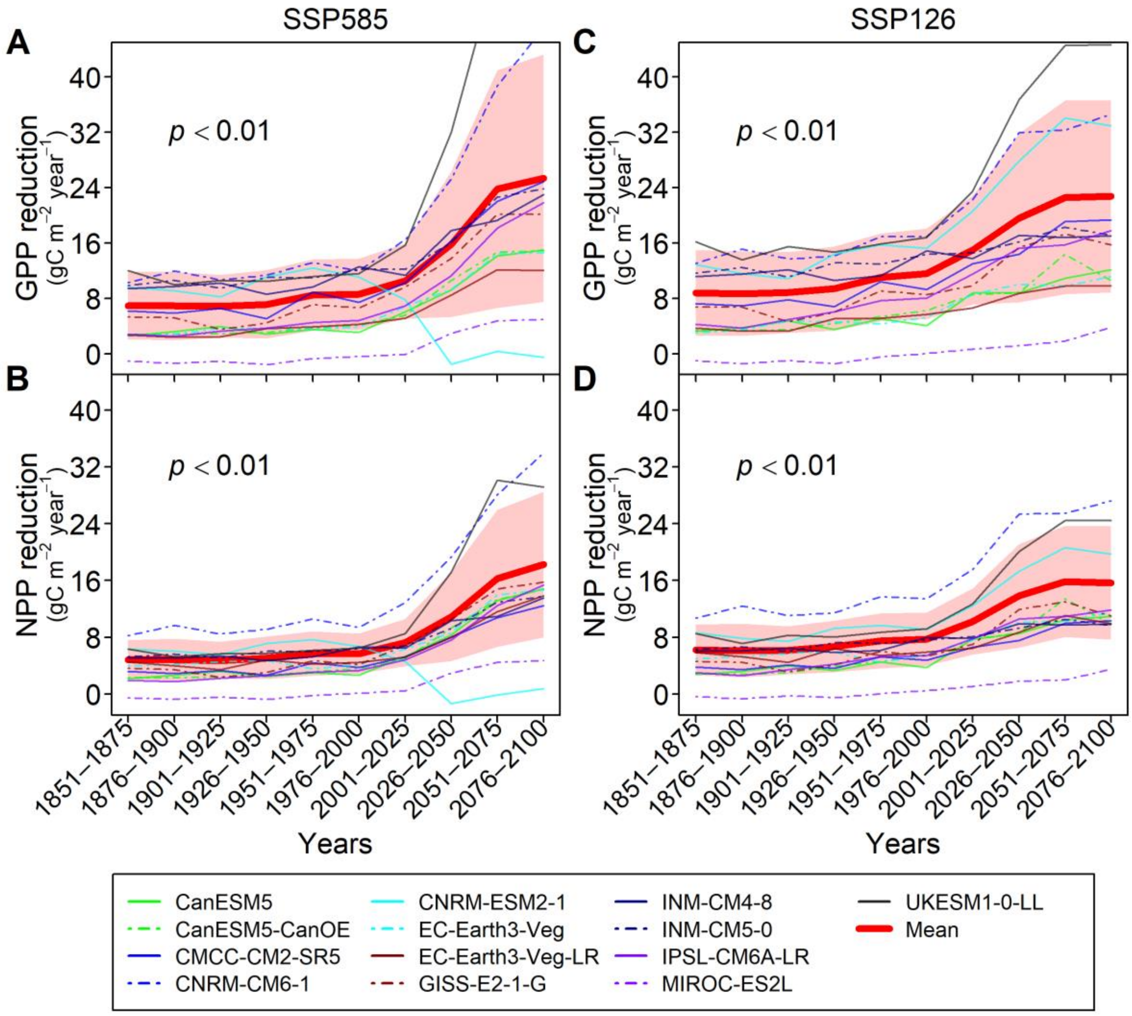

917

Figure 4

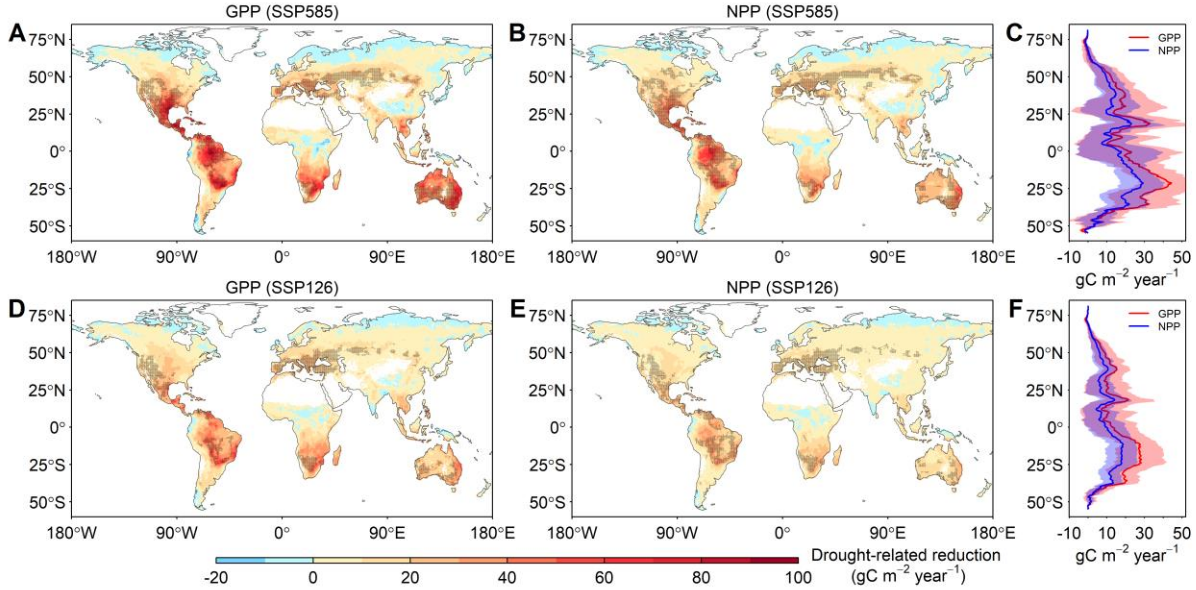
GPP (SSP585)
NPP (SSP585)
GPP (SSP126)
NPP (SSP126)
A
B
C
D
E
F
75°N
50°N
25°N
0°
25°S
50°S
180°W
90°W
0°
90°E
180°E
GPP
NPP
-10
10
30
50
gC m^{-2} year^{-1}
-20
0
20
40
60
80
100
Drought-related reduction
(gC m^{-2} year^{-1})

Figure 5

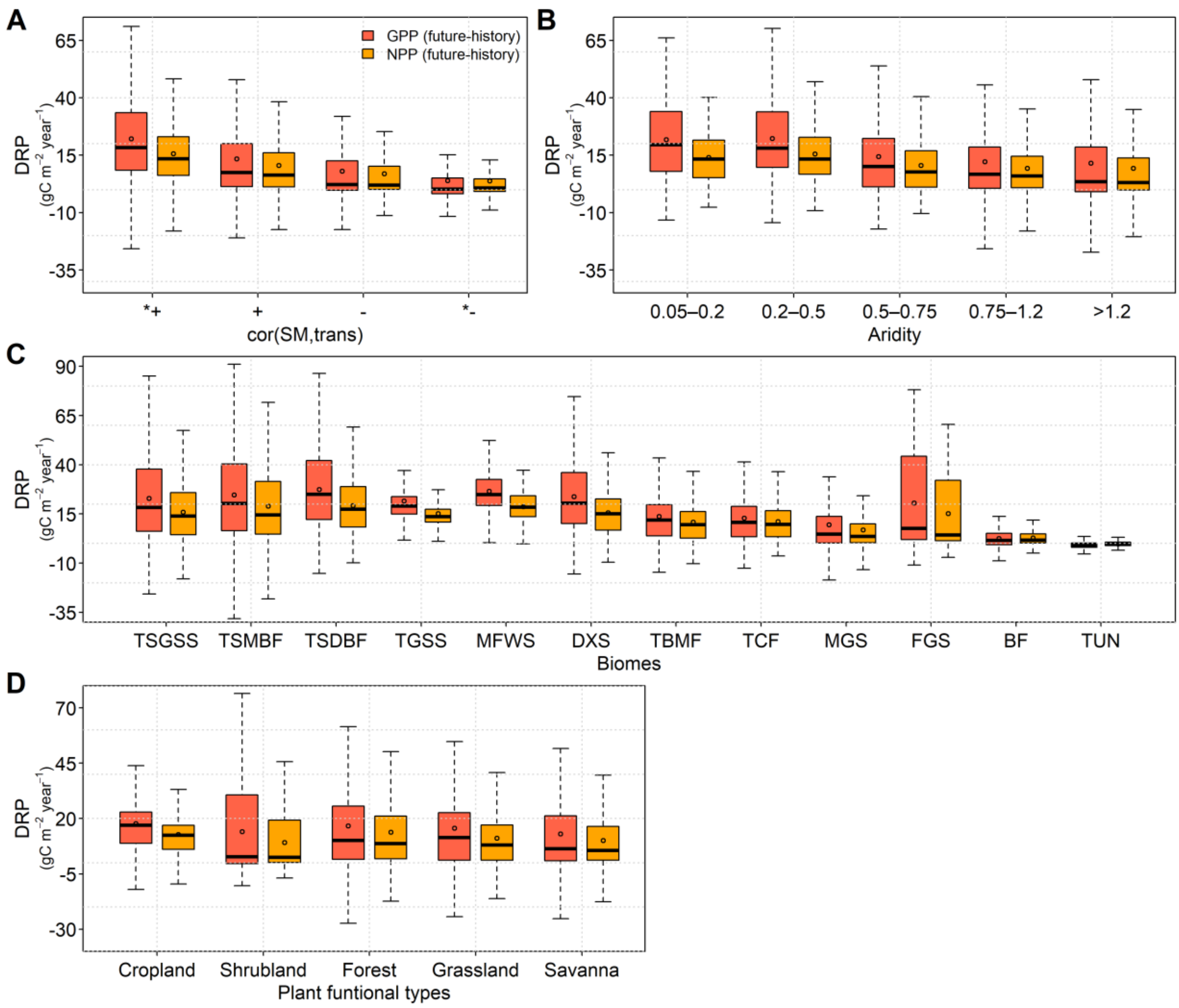
A
GPP (future-history)
NPP (future-history)
DRP
(gC m-2 year-1)
65
40
15
-10
-35
*+
+
-
*-
cor(SM,trans)
B
0.05–0.2
0.2–0.5
0.5–0.75
0.75–1.2
>1.2
Aridity
C
90
TSGSS
TSMBF
TSDBF
TGSS
MFWS
DXS
TBMF
TCF
MGS
FGS
BF
TUN
Biomes
D
70
45
20
-5
-30
Cropland
Shrubland
Forest
Grassland
Savanna
Plant funtional types

922 **Figure 6**

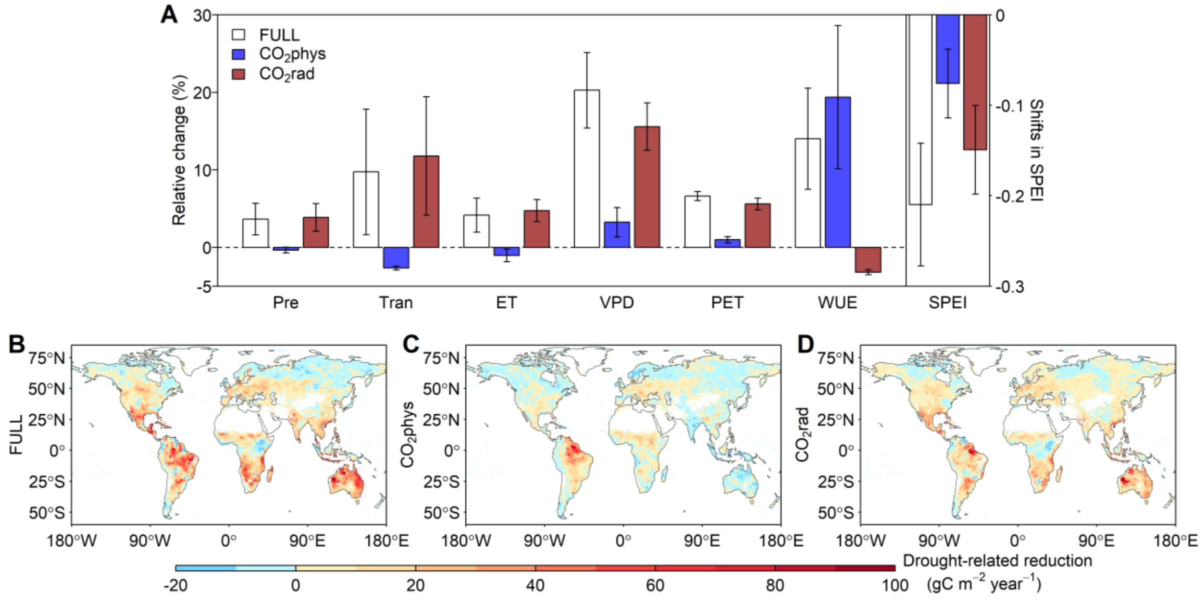

923